Proceedings of the 21st ICSMGE, Vienna, Austria, 14 – 19 June 2026. Pistrol, Adam & Schweiger (eds.)
Published by: ÖGG, Austrian Society for Geomechanics, Salzburg, Austria, ISBN 978-3-9503898-4-5
https://doi.org/10.53243/ICSMGE2026-441

Anisotropic shear strength response in Clearwater Formation Clayshales

Julian Contreras, Michael T. Hendry
Department of Civil and Environmental Engineering, University of Alberta, Edmonton, Canada, jcontrer@ualberta.ca

David Elwood
Department of Civil, Geological and Environmental Engineering, University of Saskatchewan, Saskatoon, Canada

ABSTRACT: The stress-strain response of heavily overconsolidated clay (HOC) is characteristically nonlinear and directionally dependent. Traditional evaluation of stiffness anisotropy typically relies on triaxial testing; however, the brittle nature and disturbance sensitivity of HOC materials often compromise the reliability of such methods. The Cambridge Self-boring Pressuremeter (SBPM) offers an in-situ alternative, capturing soil behavior from initial loading through yielding. Equipped with 6-axis displacement arms, the SBPM records deformations circumferentially around the borehole, enabling a comprehensive three-dimensional characterization of stiffness and shear strength across various depths and orientations. Complementary wave velocity measurements further enhance the interpretation of small-strain stiffness. This study emphasizes the Clearwater Formation Clayshale, located at Syncrude's oil sands site near Fort McMurray, Canada. It investigates the anisotropy in strength and stiffness, quantifying shear modulus degradation, in-situ lateral stress anisotropy, and undrained strength anisotropy. The findings highlight the influence of stress state on stiffness anisotropy, evaluating the response from small strains up to the elastic threshold. The analysis also considers the effects of lateral stress relief during excavation and the role of stress history in shaping anisotropic stiffness behavior. Finally, the degradation of the secant shear modulus is examined using field data, with comparisons drawn against theoretical power law relationships and a hyperbolic model.

KEYWORDS: Anisotropy, strength, stiffness, small strains, shear modulus, pressuremeter.

1 BACKGROUND INFORMATION

Anisotropy in clay soils is a complex phenomenon that has received extensive research attention because of its significant impact on three-dimensional soil behaviour. Studies demonstrate that anisotropy in clays intensifies with increasing overconsolidation ratio (OCR) (Mayne et al., 1988). In normally consolidated clays, anisotropy manifests as a function of applied stress direction and preferential particle orientation (Jardine et al., 1984, 2002). Clayton (2011) demonstrated that small-strain stiffness in normally consolidated clays varies significantly with loading direction.

In overconsolidated and highly overconsolidated (HOC) clays, anisotropy becomes more pronounced due to stress history. These materials have experienced past effective pressures exceeding current conditions, resulting in stiffer and anisotropic structures. Anisotropy in HOC clays is primarily attributed to microstructure, fissures, weakness planes, mineralogical composition, and consolidation history, directly affecting shear strength and stiffness (Smith & Johnson, 2020). These materials exhibit high sensitivity to moisture and stress variations, becoming susceptible to sliding (Yu et al., 2024), collapse, and excessive deformation when anisotropic properties are inadequately considered (Brown et al., 2019; Wong et al., 2008).

Previous investigations have addressed anisotropy through multiple approaches. Laboratory testing of undisturbed and remoulded specimens has evaluated heterogeneity, weak stratifications, and fractures (Fjær & Nes, 2014; Tien et al., 2006). Failure modes correlate closely with strain localization (Desrues & Viggiani, 2004; Zhu et al., 2016), and changes in principal stress directions may shift failure modes between localized and diffused failure modes (Zhang et al., 2021). Numerical models have been developed to assess anisotropic failure criteria in heterogeneous reservoirs (Zhang et al., 2020, 2024).

Empirical and physico-mathematical models enable stiffness parameter estimation, but practical application remains challenging due to uncertainty in anisotropic parameter determination and soil variability (Wang et al., 2022). Nowadays, knowledge gaps persist regarding in-situ anisotropy and small-strain behaviour in clayshales. Heterogeneity and discontinuities complicate intact sample acquisition and accurate laboratory data collection. Numerical modelling and laboratory or field test interpretation pose challenges due to microstructural complexity and soil variability, highlighting the need for improved research to enhance accuracy and applicability under real conditions (Davis & Miller, 2021).

Surface mining operations involving clayshales pose significant geotechnical challenges that require accurate characterization of soil mechanical properties. Traditional geotechnical analysis has predominantly relied on limit equilibrium methods focused on strength parameters; however, contemporary engineering practice increasingly demands a transition toward deformation-based modelling approaches that incorporate more complex soil behaviours. This change in approach requires understanding the relationship between stress and strain, and detailed knowledge of stiffness in order to predict the response of the ground under various loading conditions, especially in applications involving excavations where service limit states determine performance criteria.

The incorporation of advanced constitutive models requires a comprehensive characterization of stiffness parameters across different strain ranges and stress paths. Small-strain stiffness parameters are particularly critical as they govern initial deformation response and elastic behavior within the pre-yield domain. The determination of these parameters through reliable methodologies becomes essential for accurate numerical modelling and performance prediction.

1.1 *Clearwater Formation Characteristics*

The Clearwater Formation, located in northern Alberta, Canada, is a marine sequence of overconsolidated clay and shale deposited during the Cretaceous period. The Clearwater Formation is composed mainly of clayey shales interbedded with siltstone, sandstone, limestone, and bentonite (Scott and Brooker, 1968). The alternating and laminated characteristics of these deposits lend anisotropic mechanical properties to the shale sequences, wherein structural failures preferentially occur along weaker bentonitic horizons through shear displacement parallel to bedding planes. Such failure mechanisms may be attributed to stress redistributions associated with sedimentary loading, tectonic deformation, glacial processes, and erosion (Mollard, 1977).

The Clearwater Formation clayshale exhibits proven anisotropic structure through large-strain experimental investigations (Zadeh & Chalaturnyk, 2015); however, small-strain anisotropic behaviour remains unstudied. HOC clays display pre-yield strength-dominated behaviour, crucial for practical applications involving slope cuts where stress states remain below initial consolidation levels. These materials exhibit significant geotechnical challenges due to their sensitive microstructure and expansive behavior upon moisture exposure. Sample disturbance effects consistently yield reduced laboratory-derived stiffness parameters compared to in-situ measurements (Elwood, 2014). This discrepancy has highlighted the need for more reliable methods of assessing soil strength and stiffness, leading to the development of in-situ testing techniques that avoid disturbances caused during sample extraction. The Cambridge self-boring pressuremeter has proven valuable, offering high-resolution stress-strain data directly from the field environment (Byrne & Elwood, 2024; Contreras et al., 2023; Dreger et al., 2024).

This study assesses the anisotropic response of the strength and stiffness of the Clearwater Formation clayshale using a self-boring pressuremeter, evaluating in-situ lateral stress and yield, as well as undrained strength and shear modulus degradation prior to yield. The results of this research will complement the little-known characteristics of the Clearwater Formation clayshale and provide a better understanding of the behavior of highly overconsolidated materials in a range of small strains and up to yield.

1.2 *Data Collection*

This research used in-situ testing data from the Aurora North Ground Investigation 2021 and 2022 developed by the University of Saskatchewan, ConeTec Investigations Ltd and Cambridge Insitu at the Aurora North Mine of Syncrude Canada Ltd. (SCL) in Alberta, Canada (see Figure 1).

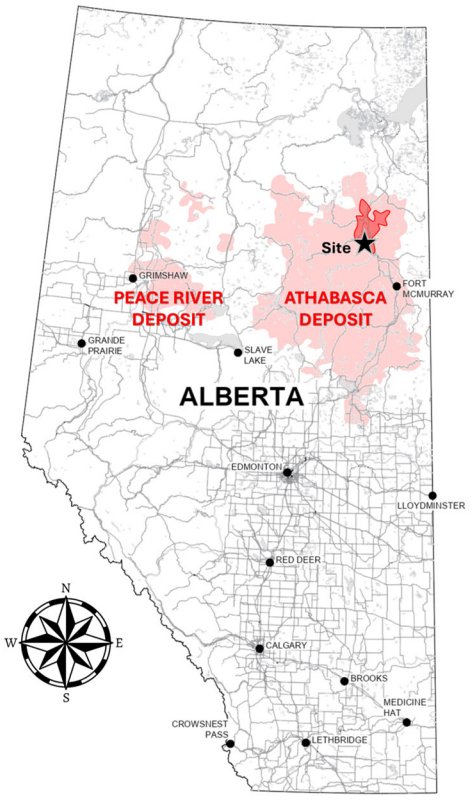

Figure 1. Location map of main heavy-oil and bitumen deposits, Alberta, Canada

Five pressuremeter tests were conducted in the Clearwater clayshale layer using the self-borehole probe (SBPM) in borehole 21-7002 and 22-7030; the depth and test characteristics are shown in Table 1.

Table 1. Details of tests carried out

Borehole	Test	Layer	Depth (mBGL)	Elevation (mASL)	Max Pressure (kPa)
21-7002	Test 6	KCA	42.05	247.60	3417
22-7030	Test 1	KCB	24.70	263.90	1811
22-7030	Test 2	KCB	26.47	262.13	4537
22-7030	Test 3	KCA	29.70	258.90	2383
22-7030	Test 4	KCA	31.66	256.94	4478

Based on the number of SBPM tests available, borehole 22-7030 is taken as a reference (see Figure 2); however, the results of test 6 of borehole 21-7002 will also be discussed throughout this paper.

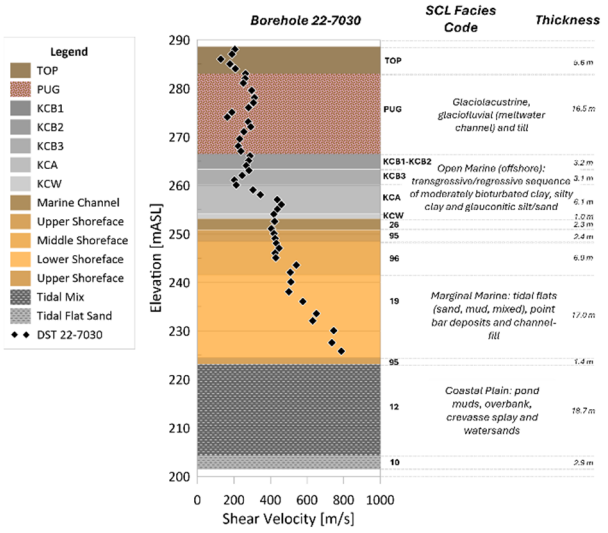

Figure 2. Stratigraphy of borehole 22-7030.

1.3 *Self-Boring Pressuremeter Testing*

The pressuremeter instrument used was designed and manufactured by Cambridge Insitu Ltd. The self-bore pressuremeter test (SBPM) has an outer diameter of 88 mm and a test interval length of approximately 0.5 m, the test features a data log every 6 seconds and 2 unload and reload cycles were performed during probe expansion and one unload-reload cycle during contraction.

The probe has 6 arms distributed in 3 different axes; in this investigation, the cavity is assumed to expand anisotropically in each axis, with a displacement per axis corresponding to the average pair of arms in each axis. Figure 3 shows the cavity expansion for test 2, with the maximum displacements of arm pairs 1-4, 2-5, and 3-6.

A vertical view of the borehole is shown in Figure 3, where the cavity radius (a), equivalent to half the borehole diameter of the SBPM probe, can be visualized. The test starts with applying pressure and an expansion of the probe, the arms start the displacement once the pressure exceeds the in-situ lateral stress, σ_h *or* P_0. The soil is loaded and obtains an elastic response up to the failure point, then plastic behaviour in the

cavity wall (c) and an elastic behaviour in the soil away from the cavity wall (b) are obtained; this process is carried up to a point of maximum displacement.

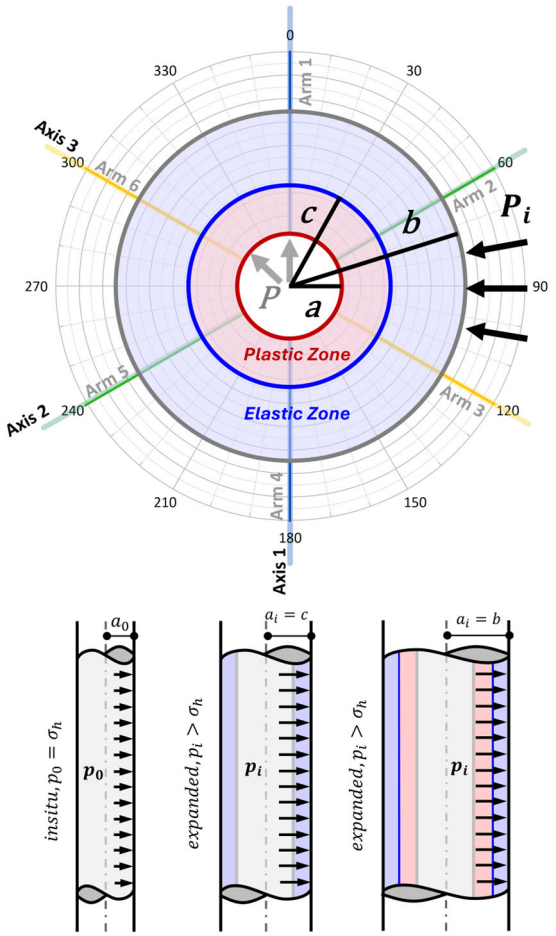

Figure 3. Cylindrical cavity expansion theory.

Once the point of maximum displacement is reached, the probe is unloaded, i.e., a cavity contraction process is initiated. The contraction process is opposite to the expansion process. In this process, the data are slightly less disturbed, so the undrained strength measurement is more reliable during unloading than reloading.

In the present study, the calculation of the undrained strength is based on the analysis of the elastic response. Therefore, the nonlinear behavior of plasticity is not considered, and the stress state beyond the yielding point is not studied.

2 ANISOTROPIC RESPONSE

Although the basic considerations for developing the elastoplastic models assume isotropic properties, the Cambridge pressuremeter has great potential to measure the cavity's deformation from its arms' displacements. Six arms are distributed in 3 axes for the self-boring pressuremeter, measuring the stress-strain behaviour in the 360° of the cavities. The probe pressure is the same for the 3 axes. Therefore, the test becomes a controlled stress test, with a particular displacement response for each axis. Pressuremeter tests generally consider the average of their arms to define the stress-strain behaviour because the reference of the displacements is the body of the instrument itself. In the case of considering separate axes, it would be assumed that the instrument remains rigid. In the case of the self-borehole pressuremeter (SBPM), it is considered that the membrane and the arms are in direct contact with the cavity, so each arm must detect the soil reaction according to the stiffness of its structure on each axis.

Figure 4 shows the response of the applied pressure to the displacement of the cavity for test 3 of borehole 7030. Here, each axis presents an independent response associated with the stiffness of the soil in each direction. Noticeably, under the same cavity pressure, one axis obtains greater displacement than the other two, clearly marking the area of lower stiffness. This is the initial response to possible anisotropic behaviour. However, the in-situ lateral stress response, yield stress, undrained strength, and shear modulus were evaluated in greater detail.

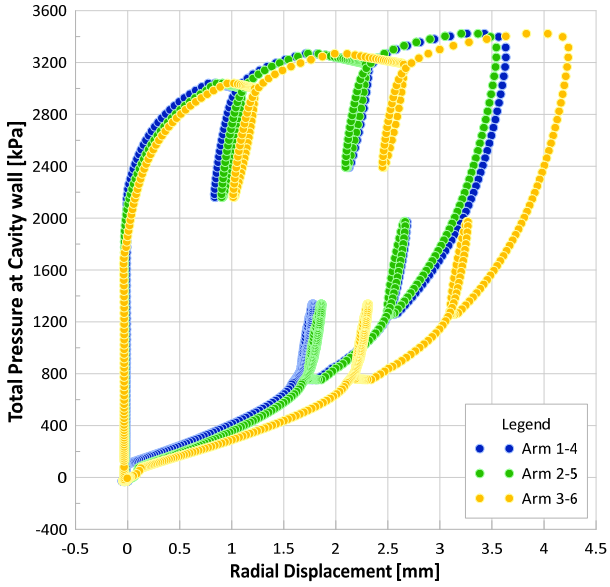

Figure 4. Response of Borehole 7030-T3.

2.1 *In-situ Lateral Stress, P_0*

In-situ lateral stress was evaluated using the Lift-off Method and the nonlinear elastic pore water pressure (PWP) response. The Lift-off Method is particularly effective with the SBPM, as its self-boring nature ensures direct membrane contact with the cavity wall, minimizing initial measurement distortion and identifying the onset of radial displacement, interpreted as in-situ lateral stress. Our findings indicate that the average arm response reflects the dominant axis, excluding zones of higher resistance (see Figure 5).

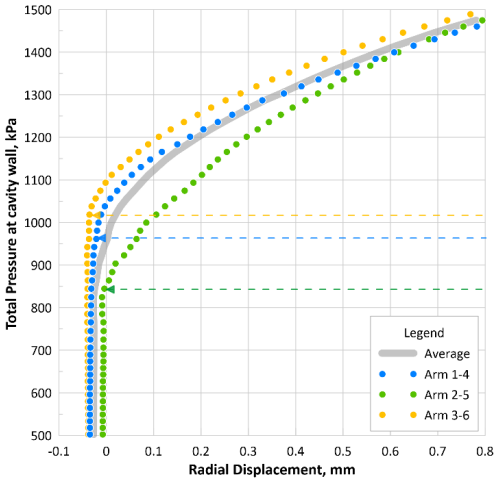

Figure 5. Lift-off Response of Borehole 7030-T1.

Clarke (1993) first highlighted the variability in 3-arm pressuremeter readings, cautioning that probe inclination could introduce vertical stress components. In our study, probe verticality was monitored, and data were processed considering the average of the arms per axis; in this way, the response obtained is limited to the cavity pressure in the three axes.

On the other hand, the PWP Method (Bolton & Whittle, 1999) calculates lateral stress based on the initial rise in pore pressure (see Figure 6). However, this approach is limited by its isotropic nature; PWP sensors capture an averaged response and cannot resolve directional anisotropy. Unlike arm-based measurements, which reflect orientation-specific behaviour, pore pressure readings respond to the lowest principal stress, providing a less detailed interpretation of anisotropic soil conditions.

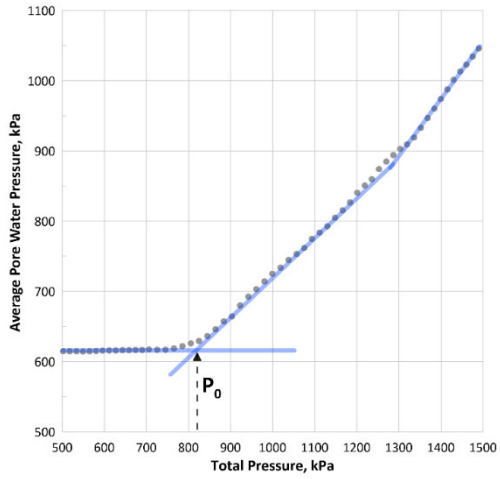

Figure 6. Porewater Pressure (PWP) Response

Figure 7 shows the in-situ lateral stress distribution for 7030-T1. The lower principal stress of the Lift-off method matches the response of the PWP Method. The Lift-off method shows a marked anisotropy, with a difference of 200 kPa between the lowest and highest principal stress.

Figure 7. Anisotropic Initial Pressure (P_0) Test 7030-T1

2.2 *In-situ Yield Stress, P_Y*

The initial yield stress correlates with in-situ yield conditions. This study employed the Marsland and Randolph (1978) method alongside a Non-linear Elastic Pore Pressure Response model. While anisotropy is less pronounced than lateral in-situ stress, minor anisotropy is evident (see Figure 8). The PWP method yields an isotropic response, averaging the principal stresses from the Marsland and Randolph approach. Results indicate isotropic stress behaviour at yielding. Overall, yield stress variations are minimal, implying that the formation's stress history is predominantly transversely isotropic. Table 2 summarizes the lateral stress and in-situ yield stress values obtained for each axis.

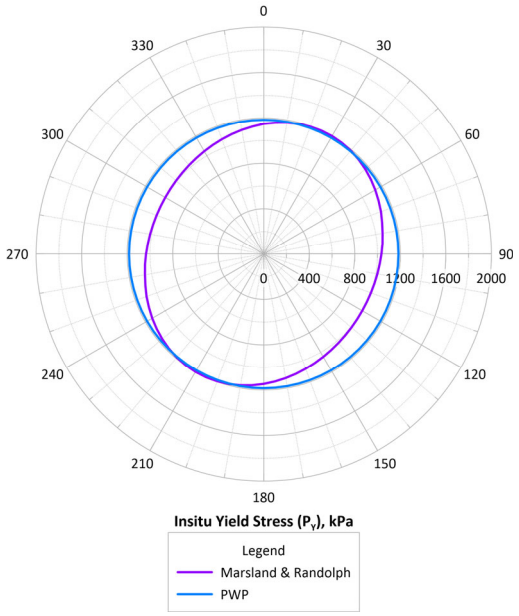

Figure 8. Anisotropic In-situ Yield Stress (P_Y) Test 7030-T1

Table 2. Insitu Lateral Stress and Insitu Yield Stress

Test	Axis	P_0		P_Y	
		Lift Off	PWP	M&R	PWP
22-7030-T1	Axis 1	1018.7	824.7	1148.1	1183.8
	Axis 2	999.5	824.7	1130.0	1183.8
	Axis 3	824.7	824.7	999.5	1183.8
22-7030-T2	Axis 1	1168.8	573.0	1631.7	1593.9
	Axis 2	529.9	573.0	1593.9	1593.9
	Axis 3	573.0	573.0	1593.9	1593.9
22-7030-T3	Axis 1	753.0	700.6	1457.3	1237.6
	Axis 2	753.0	700.6	1237.6	1237.6
	Axis 3	753.0	700.6	1186.4	1237.6
22-7030-T4	Axis 1	949.2	858.3	1747.8	1747.8
	Axis 2	903.6	858.3	1697.9	1747.8
	Axis 3	949.2	858.3	1697.9	1747.8
21-7002-T6	Axis 1	2183.8	1352.0	2455.1	2108.8
	Axis 2	1859.9	1352.0	2108.8	2108.8
	Axis 3	1649.2	1352.0	2108.8	2108.8

2.3 *Undrained Shear Strength, S_u*

Undrained strength was estimated using the approaches of Palmer (1972), Jefferies (1988), and Gibson and Anderson (1961). While Palmer and Gibson & Anderson assess strength

during the expansion phase, Jefferies evaluates it during unloading or compression. All methods yield comparable results; however, the Gibson & Anderson (1961) method more effectively captures anisotropy. This is due to the clearer trend observed in the logarithmic shear strain during loading. Figure 9 illustrates the anisotropic response of undrained strength in Test 1 from borehole 7030.

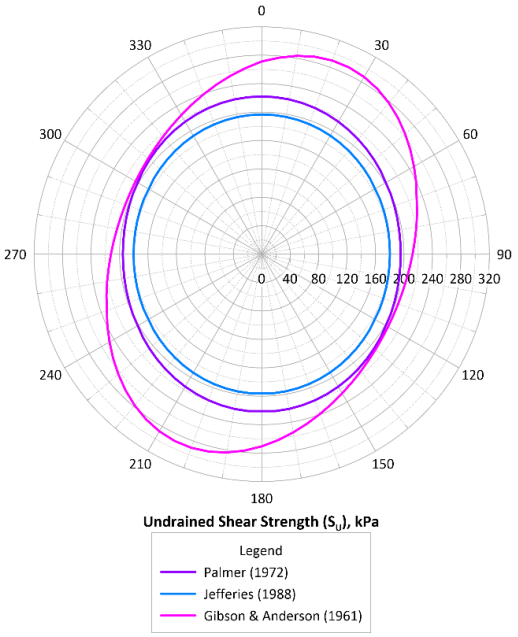

Figure 9. Anisotropic Undrained Shear Strength (S_u) Test 7030-T1.

3 STIFFNESS

3.1 *Secant Shear Modulus, G_s*

One of the key contributions of this study is the evaluation of stiffness anisotropy. Shear stress and strain were analyzed to determine the secant shear modulus (Gs) within the shear plane (τ–γ), rather than within the cavity's stress-strain space. Gs was computed at each measurement point, leveraging the Cambridge pressuremeter's high sensitivity to displacement during unloading-reloading cycles. This enabled precise characterization of small-strain behavior. The initial reload point was manually defined following Bolton and Whittle (1999), identifying the minimum shear stress during unloading and fitting the corresponding stress to the non-linear power law trend. This procedure was applied across all three test axes, yielding secant shear modulus and shear strain values directly from field data. As shown in Figure 10, the initial shear modulus progressively decreases as yielding is approached, illustrating modulus degradation. Table 3 summarizes the undrained shear strength values and the degraded shear modulus.

Table 3. Undrained Shear Strength and Shear Modulus

Test	Axis	S_u			Shear Modulus			
		Pal.	Jef.	GA	G_0 (0.001%)	G_s (0.01%)	G_s (0.1%)	G_s (1%)
22-7030-T1	Axis 1	222	197	271	82	82	58	27
	Axis 2	202	185	246	55	55	50	20
	Axis 3	202	184	205	45	45	39	18
22-7030-T2	Axis 1	763	897	898	231	231	142	60
	Axis 2	710	888	898	200	200	138	62
	Axis 3	702	786	898	171	171	130	61
22-7030-T3	Axis 1	290	314	356	175	157	115	35
	Axis 2	282	304	317	134	133	101	34
	Axis 3	281	290	275	138	132	102	33
22-7030-T4	Axis 1	1022	314	356	321	321	175	71
	Axis 2	987	304	317	297	297	163	66
	Axis 3	903	290	275	235	235	160	62
21-7002-T6	Axis 1	1022	964	924	273	230	158	51
	Axis 2	987	864	899	213	199	153	54
	Axis 3	903	839	824	207	195	148	47

3.2 *Shear Modulus Degradation*

At this point, the degradation of the shear modulus, measured from data obtained directly in the field, was modeled graphically using three approaches: the power law of Bolton and Whittle (1999), the hyperbolic model proposed by Habert and Lopes (2024), and a recently introduced sigmoidal model. These models were selected to capture the nonlinear behavior of stiffness reduction as deformation increases. The mathematical formulations of each model are presented below:

$$G_s = G_r + \frac{(G_0 - G_r)}{\left[1 + \left(\gamma_n / a\right)^n\right]^m} \quad (1)$$

$$G_s = \frac{G_0}{1 + \left(G_0 \cdot \gamma / S_u\right)} \quad (2)$$

$$G_s = \alpha \gamma_c^{\beta - 1} \quad (3)$$

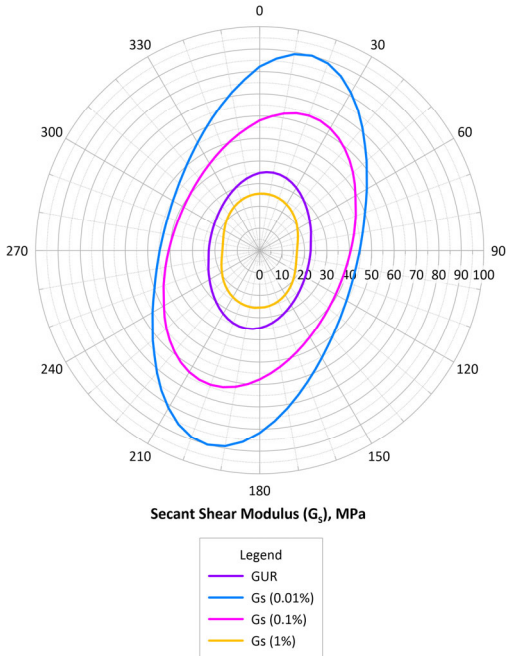

Figure 10. Anisotropic Secant Shear Modulus (G_s) Test 7030-T1.

The hyperbolic model operates the initial shear modulus (G_0) following the methodology outlined by Lopes (2024), whereas the sigmoidal model defines G_0 based on the natural inverse trend of shear strain. Additionally, G_0 obtained from Downhole Seismic Testing (DST) was used as a reference. However, current findings do not conclusively establish the

shear strain range captured by DST relative to the SBPM operational range. Figure 11 presents the average modulus degradation across SBPM axes, demonstrating that both the sigmoidal and hyperbolic models effectively represent a significant portion of secant shear modulus reduction. In contrast, the power law model accurately represents near the yield point (approximately 1% shear strain). The secant shear modulus was calculated individually for each pressuremeter axis to evaluate anisotropy in modulus degradation. The results show significant anisotropy at low strain levels, which decreases as yielding is approached. As illustrated in Figure 11, the soil exhibits strong directional stiffness behaviour under low strain, transitioning to isotropic stiffness near the yield threshold.

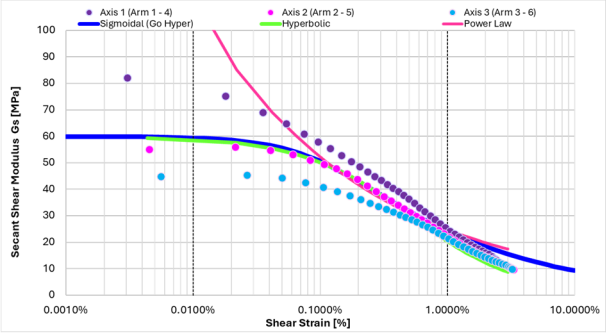

Figure 11. Shear Modulus Degradation Anisotropic Response.

4 CONCLUSIONS

This investigation demonstrates that the Cambridge Self-boring Pressuremeter effectively characterizes anisotropic behaviour in Clearwater Formation clayshales, overcoming traditional limitations of laboratory testing in heavily overconsolidated clays. The study reveals pronounced anisotropy in in-situ lateral stress, with variations up to 200 kPa between principal stress directions, while yield stress exhibits minimal directional dependency, indicating predominantly transversely isotropic stress history. Most significantly, secant shear modulus degradation analysis shows substantial stiffness anisotropy at small strains that progressively diminishes approaching yield conditions, transitioning from highly directional behavior to near-isotropic response. The sigmoidal and hyperbolic models successfully capture modulus degradation trends, with the power law model proving most accurate near yield threshold (≈1% shear strain). These findings provide critical insights for geotechnical design in oil sands applications, establishing that anisotropic considerations are essential for accurate small-strain stiffness assessment in clayshale formations.

5 ACKNOWLEDGEMENTS

This research has been carried out as part of an NSERC Alliance Grant supported by Syncrude Canada Ltd., ConeTec Investigations Ltd and Cambridge In-Situ Ltd. The researchers at the University of Saskatchewan and the University of Alberta would like to thank all participants. Pressuremeter testing was carried out by Cambridge In-situ and ConeTec, Downhole Seismic testing was carried out by ConeTec.

6 REFERENCES

Bolton, M. D., & Whittle, R. W. (1999). A non-linear elastic/perfectly plastic analysis for plane strain undrained expansion tests. Géotechnique, 49(1), 133-141.

Brown, A., Smith, J., & Davis, R. (2019). Stability analysis of overconsolidated clay slopes: Effects of anisotropy. Journal of Geotechnical Engineering, 45(3), 234-248.

Byrne, Y., and Elwood, D. (2024). Characterizing non-linear elastic behavior in soils and soft rock: insights from high-resolution pressuremeter testing. In Proceedings of the 17th Pan-American Conference on Soil Mechanics and Geotechnical Engineering (XVII PCSMGE), and 2nd Latin-American Regional Conference of the International Association for Engineering Geology and the Environment (IAEG), La Serena Chile, 2024

Clarke, B. G. (1993). Pressuremeters in geotechnical design. Blackie Academic & Professional.

Clayton, C. R. I. (2011). Stiffness at small strain: Research and practice. Géotechnique, 61(1), 5-37.

Contreras, J., Manderson, A., Hendry M., Elwood D., Byrne, Y. (2023). Comparison of the nonlinear modulus of the Cambridge self-boring pressuremeter in Clearwater Formation Clayshales. In Proceedings of the 76th Canadian Geotechnical Conference GeoSaskatoon 2023.

Coolidge, M. (2016). Oil sands development in Alberta: Environmental and economic perspectives. Canadian Energy Journal, 12(4), 45-62.

Davis, L., & Miller, K. (2021). Challenges in characterizing heterogeneous clay formations. Geotechnical Testing Journal, 44(2), 289-304.

Dreger, C., Byrne, Y., Martin, C.D., Elwood, D., Senft, D., Stevenson, G., and Watson, A.D. (2024). High Pressure Pressuremeter Tests in the Shaftesbury Shales at the Site C Project. In Proceedings of the 77th Canadian Geotechnical Conference, GeoMontreal 2024, Montreal, QC.

Elwood, D. (2014). In-situ testing of overconsolidated clays: A comparative study. Canadian Geotechnical Journal, 51(8), 892-905.

Gibson, R. E., & Anderson, W. F. (1961). In situ measurement of soil properties with the pressuremeter. Civil Engineering and Public Works Review, 56(658), 615-618.

Habert, J., & Lopes, F. R. (2024). Hyperbolic model for shear modulus degradation in clays. Soil Dynamics and Earthquake Engineering, 178, 108-119.

Jardine, R. J., Potts, D. M., Fourie, A. B., & Burland, J. B. (1984). Studies of the influence of non-linear stress-strain characteristics in soil-structure interaction. Géotechnique, 34(3), 377-396.

Jefferies, M. G. (1988). Determination of horizontal geostatic stress in clay with self-bored pressuremeter. Canadian Geotechnical Journal, 25(3), 559-573.

Lopes, F. R. (2024). Advanced interpretation methods for pressuremeter testing in clays. Geotechnical Engineering Journal, 67(2), 145-162.

Marsland, A., & Randolph, M. F. (1978). Comparisons of the results from pressuremeter tests and large in situ plate tests in London Clay. Géotechnique, 28(2), 147-170.

Mayne, P. W., Kulhawy, F. H., & Trautmann, C. H. (1988). Laboratory modeling of laterally-loaded drilled shafts in clay. Journal of Geotechnical Engineering, 114(9), 1017-1035.

Mollard, J. D. (1977). Regional landslide types in Canada. Geological Survey of Canada Paper, 77-1A, 29-35.

Palmer, A. C. (1972). Undrained plane-strain expansion of a cylindrical cavity in clay: A simple interpretation of the pressuremeter test. Géotechnique, 22(3), 451-457.

Scott, J. S., & Brooker, E. W. (1968). Geological and engineering characteristics of glacial lake clays in western Canada. Geological Society of America Bulletin, 79(9), 1187-1200.

Smith, P., & Johnson, R. (2020). Microstructural controls on anisotropy in overconsolidated clays. Clay Minerals, 55(2), 134-148.

Wang, L., Chen, Y., & Liu, X. (2022). Uncertainty quantification in anisotropic soil parameter estimation. Computers and Geotechnics, 149, 104-118.

Whittebolle, B. I. F. (1982). Sample disturbance in clay soils. Ground Engineering, 15(4), 21-25.

Wong, R. C. K., Chau, K. T., & Tang, C. A. (2008). Analysis of crack coalescence in rock-like materials containing three flaws. International Journal of Rock Mechanics and Mining Sciences, 38(7), 909-924.

Yu, X., Zhao, T., Gong, B. & Tang, C. (2024). The water weakening effect on the progessive slope failure under excavation and rainfall conditions. Bulletin of Engineering Geology and the Environment

Zadeh, M. K., & Chalaturnyk, R. J. (2015). An experimental study of the mechanical behavior of a clay shale. International Journal of Rock Mechanics and Mining Sciences, 75, 192-201.